Hindawi
Advances in Astronomy
Volume 2018, Article ID 2417939, 7 pages
https://doi.org/10.1155/2018/2417939

Research Article

Poisson Denoising for Astronomical Images

Fahad Shamshad,[1] M. Mohsin Riaz,[2] and Abdul Ghafoor[1]

[1]*Military College of Signals, National University of Sciences and Technology, Pakistan*
[2]*Center for Advanced Studies in Telecommunication, COMSATS Islamabad, Pakistan*

Correspondence should be addressed to Abdul Ghafoor; abdulghafoor-mcs@nust.edu.pk

Received 12 February 2018; Revised 5 April 2018; Accepted 23 April 2018; Published 10 June 2018

Academic Editor: Wing-Huen Ip

A denoising scheme for astronomical color images/videos corrupted with Poisson noise is proposed. The scheme employs the concept of Exponential Principal Component Analysis and sparsity of image patches. The color space RGB is converted to YCbCr and K-means++ clustering is applied on luminance component only. The cluster centers are used for chromatic components to improve the computational efficiency. For videos, the information of both spatial and temporal correlations improves the denoising. Simulation results verify the significance of proposed scheme in both visual and quantitative manner.

1. Introduction

Recent advancements in astronomy and digital systems emphasize the development of more sophisticated image processing algorithm. Acquisition of astronomical images in low photon count region is a dominant source of Poisson noise. The images containing intensity dependent Poisson noise (having same mean and variance value) cannot be accurately modelled with Gaussian distribution.

In [1], Poisson noise is converted into Gaussian noise with unit variance using Variance Stabilization Transform (VST). Further improvement is made by applying Bayesian multiscale likelihood models [2] and l_1 penalization hypothesis testing [3]. However these schemes [1–3] provide significantly degraded results for high Poisson noise. Close form approximation for unbiased inverse of Anscombe transform yields increased error peak for Poisson noise [4, 5]. Structured dictionary learning approach exploiting the self-similarity of image patches [6] requires significant amount of computational time especially for color images and videos.

In [7], multiscale Poisson denoising based on shrinkage operators to attain maximum l_2 error is proposed. However l_2 distance is not suitable for Poisson corrupted measurements. In [8] spatially adaptive total variation framework is proposed with split Bregman optimization for Poisson denoising to handle high computational load but yields poor results in low photon count regime which is usually the case with astronomical images. Directional lapped orthogonal transform overcomes the limitation of diagonal edges and textures which separable wavelets fail to denoise efficiently [9]. Computationally efficient technique for estimation of unknown noise parameters requires a blank image under same mechanical shutter [10]. In a nutshell, most of above-mentioned techniques either suffer from high computational complexity or give poor results in high Poisson noise.

A denoising scheme for astronomical color images/videos corrupted with Poisson noise is proposed. The scheme first converts the color space from RGB to YCbCr and applies K-means++ clustering on luminance component only. The same cluster centers are used for chromatic components to improve the computational efficiency. Framework of Exponential Principal Component Analysis (EPCA) [11] is employed that better suits high Poisson noise. The proposed algorithm addresses several drawbacks of existing schemes while ingeriting their main strengths. For instance, patch based approach is used to exploit redundancies in image that have been shown to improve performance of image denoising algorithms [6]. Similarly clustering algorithms are used in different denoising algorithms to group similar patches together [5]. Note that careful clustering has significant importance in case of high Poisson noise (where only few photons are acquired by detector). Similarly taking into account temporal correlation of videos also improves the performance of restoration algorithms [12, 13]. Simulation results on different images and

videos verify the significance of proposed scheme in both visual and quantitative manner.

2. Proposed Technique

Let N^{β} be the observed image from image acquisition device having dimensions $P \times Q$, where $p = 1, 2, \ldots, P$ are rows, $q = 1, 2, \ldots, Q$ are columns, and $\beta \in \{\text{red, green, blue}\}$ are color bands. For $l\epsilon\{1, \ldots, PQ\}$ let $N^{\beta}[l]$ (column stack representation of N^{β}) be the observed pixel at location i whose entries are independent Poisson random variables with true value $I^{\beta}[l] > 0$ which is to be estimated. Given the clean image $I^{\beta}[l]$ likelihood of observing noisy Poisson image $N^{\beta}[l]$ can be written as

$$\mathrm{P}\left(N^{\beta}[l] \mid I^{\beta}[l]\right) = \frac{\exp\left(-I^{\beta}[l]\right)\left(I^{\beta}[l]\right)^{N^{\beta}[l]}}{N^{\beta}[l]!} \tag{1}$$

Noisy image is converted into luminance chrominance (YCbCr) color space by matrix transformation as

$$\begin{bmatrix} N^{Y} \\ N^{Cb} \\ N^{Cr} \end{bmatrix} = \begin{bmatrix} 0.299 & 0.587 & 0.114 \\ -0.147 & -0.289 & 0.436 \\ 0.615 & -0.515 & -0.100 \end{bmatrix} \begin{bmatrix} N^{R} \\ N^{G} \\ N^{B} \end{bmatrix} \tag{2}$$

Let N^{α} denote the noisy image in YCbCr color space where $\alpha\epsilon\{Y, Cb, Cr\}$; then matrix M^{Y} of vectorized patches is constructed from the N^{Y} component by extracting all overlapping patches O of size $\sqrt{E} \times \sqrt{E}$ as

$$M^{Y} = \begin{pmatrix} N^{Y}_{1,1} & N^{Y}_{1,2} & \cdots & N^{Y}_{1,E} \\ N^{Y}_{2,1} & N^{Y}_{2,2} & \cdots & N^{Y}_{2,E} \\ \vdots & \vdots & \ddots & \vdots \\ N^{Y}_{O,1} & N^{Y}_{O,2} & \cdots & N^{Y}_{O,E} \end{pmatrix} \tag{3}$$

where $N^{Y}_{i,j}$ represents j^{th} pixel in i^{th} patch for $1 \le i \le O$ and $O = (P - \sqrt{E} + 1)(Q - \sqrt{E} + 1)$ (considering image border issues) and let $I^{Y}_{i,j}$ be defined for clean image as $N^{Y}_{i,j}$ for noisy one. Similarly matrices M^{Cb} and M^{Cr} are built for N^{Cb} and N^{Cr}, respectively.

K-means++ algorithm (having more accuracy and efficiency as compared to conventional k-means) is then applied on matrix M^{Y} to obtain clusters $c = 1, 2, \ldots, C$ and denote S_c for the size of cth cluster. As N^{Y} (luminance component) contains most of the valuable information (edges, shades, texture, etc.) of image the same cluster centers are then assigned to Cb and Cr components for computational efficiency of algorithm.

Different algorithms have used PCA to project the extracted noisy image patches to low dimensional space. Let $I^{\alpha}_{i_c,j}$ be the j^{th} pixel of i^{th} patch in cluster c; using PCA it can be written as

$$I^{\alpha}_{i_c,j} \approx (\phi\psi)^{\alpha}_{i_c,j} \tag{4}$$

where ϕ is coefficient matrix of size $S_c \times L$ and ψ is dictionary atom matrix of size $L \times E$. S_c is cluster size (patches in cluster c) and L is number of principal axes to be retained. However, in this paper, the framework of [11] is used as it is more suitable for exponentially distributed data. Equation (4) can be written as

$$I^{\alpha}_{i_c,j} \approx \exp\left(\phi\psi\right)^{\alpha}_{i_c,j} \tag{5}$$

where the exponential operator is element-wise.

After neglecting the constant term and applying maximization of negative Poisson likelihood alongwith approximation of (5), the loss function for c^{th} cluster is

$$\text{Loss}\,(U, V) = \min_{\phi,\psi} \sum_{i=1}^{S_c} \sum_{j=1}^{E} \exp\left(\phi\psi\right)^{\alpha}_{i_c,j} - N^{\alpha}_{i_c,j}\left(\phi\psi\right)^{\alpha}_{i_c,j} \tag{6}$$

Equation (6) is solved using fast Newton method [14], where ϕ and ψ are initialized randomly. Then i^{th} rows of ϕ (denoted as $\phi_{i_c,:}(t)$) at iteration t) for cluster c are updated as

$$\begin{aligned} \phi_{i_c,:}(t+1) = \phi_{i_c,:}(t) - \left(\exp\left(\phi(t)\,\psi(t)\right)_{i_c,:} - N_{i_c,:}\right) \\ \cdot \psi^{T}(t)\left(\phi(t)\,X_i\phi^{T}(t)\right)^{-1} \end{aligned} \tag{7}$$

where $X_i = \text{diag}(\exp(\phi(t)\psi(t))_{i_c,1}, \exp(\phi(t)\psi(t))_{i_c,2}, \ldots, \exp(\phi(t)\psi(t))_{i_c,E})$ is diagonal matrix of size $E \times E$ for cluster c and α is omitted for simplicity. Similarly columns of ψ (denoted as $\psi_{:,j}(t)$) are updated as

$$\begin{aligned} \psi_{:,j}(t+1) = \psi_{:,j}(t) - \left(\phi^{T}(t+1)\,D_j\phi(t+1)\right)^{-1} \\ \cdot \phi^{T}(t+1) \\ \cdot \left(\exp\left(\phi(t+1)\,\psi(t)\right)_{:,j} - N_{:,j}\right) \end{aligned} \tag{8}$$

where $D_j = \text{diag}(\exp(\phi(t+1)\psi(t))_{1_c,j}, \text{diag}(\exp(\phi(t+1)\psi(t))_{2_c,j+1}, \ldots, \exp(\phi(t+1)\psi(t))_{S_c,E})$.

Row of ϕ and columns of ψ are updated iteratively. Stopping criteria for proposed algorithm are either number of iterations (maximum 20) or a defined error threshold (0.01), whichever is reached first. Equation (6) after solving reduces to

$$\left(\widehat{\Phi}, \widehat{\Psi}\right) = \underset{(\phi,\psi)}{\text{argmin}}\ \text{Loss}\,(U, V) \tag{9}$$

and denoising estimate for cluster c is (I is clean original image while $\widehat{I}$ is denoised image)

$$\widehat{I}^{\alpha}_{i_c,j} = \exp\left(\widehat{\Phi}\widehat{\Psi}\right)^{\alpha}_{i_c,j} \tag{10}$$

After denoising of all c clusters, denoised patches are projected onto pixels. As each pixel has multiple presentation in different patches, it is done by uniformly averaging all estimates of those patches containing given pixel. Denoising image $\widehat{I}^{\alpha}$ is then converted to RGB domain $\widehat{I}^{\beta}$ as

$$\begin{bmatrix} \widehat{I}^{R} \\ \widehat{I}^{G} \\ \widehat{I}^{B} \end{bmatrix} = \begin{bmatrix} 1 & 0 & 1.140 \\ 1 & -0.395 & -0.581 \\ 1 & 2.032 & 0 \end{bmatrix} \begin{bmatrix} \widehat{I}^{Y} \\ \widehat{I}^{Cb} \\ \widehat{I}^{Cr} \end{bmatrix} \tag{11}$$

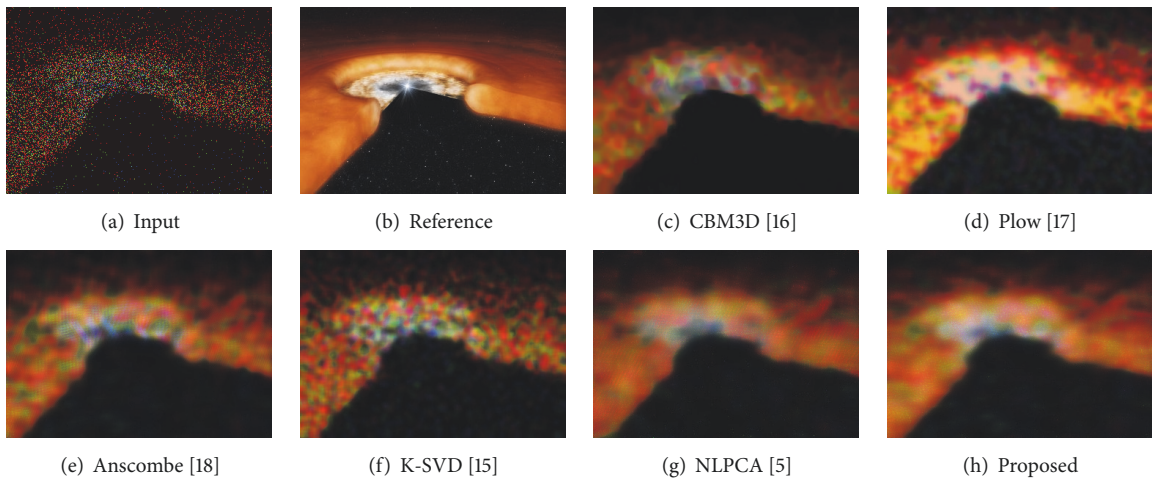

(a) Input (b) Reference (c) CBM3D [16] (d) Plow [17]

(e) Anscombe [18] (f) K-SVD [15] (g) NLPCA [5] (h) Proposed

Figure 1: Disk: noisy input, reference, and denoised images (for peak = 0.2).

The above denoising methodology is extended for Poisson noise corrupted astronomical videos by taking spatial correlation into account. Let N_t^α be Poison corrupted t^{th} frame of size $P \times Q$ in YCbCr color space where $t = 1, 2, \ldots, F$. If all overlapping cubes of size $\sqrt{E} \times \sqrt{E} \times \Lambda$ are extracted then total number of cubes will be $(P - \sqrt{E} - 1)(Q - \sqrt{E} - 1)(F - \Lambda - 1)$, where Λ represents number of frames. For simplicity denote $(P - \sqrt{E} + 1)(Q - \sqrt{E} - 1)$ by O and $(F - \Lambda + 1)$ by Z (total cubes then become $O \times Z$). After concatenating every cube row-wise, patch by patch, in single row matrix form ($N_{i,j,t}^\alpha$), j^{th} pixel of i^{th} cube in frame t is written as

$$N_{i,j,t}^\alpha = \begin{pmatrix} N_{1,1,1}^\alpha & N_{1,2,1}^\alpha & \cdots & N_{1,E,1}^\alpha & N_{1,E+1,2}^\alpha & \cdots & N_{1,E*\Lambda,\Lambda}^\alpha \\ N_{2,1,1}^\alpha & N_{2,2,1}^\alpha & \cdots & N_{2,E,1}^\alpha & N_{2,E+1,2}^\alpha & \cdots & N_{2,E*\Lambda,\Lambda}^\alpha \\ \vdots & \vdots & \cdots & \vdots & \vdots & \cdots & \vdots \\ N_{O,1,1}^\alpha & N_{O,2,1}^\alpha & \cdots & N_{O,E,1}^\alpha & N_{O,E+1,2}^\alpha & \cdots & N_{O,E*\Lambda,\Lambda+1}^\alpha \\ N_{O+1,1,2}^\alpha & N_{O+1,2,2}^\alpha & \cdots & N_{O+1,E,2}^\alpha & N_{O+1,E+1,3}^\alpha & \cdots & N_{O+1,E*\Lambda,\Lambda+1}^\alpha \\ \vdots & \vdots & \cdots & \vdots & \vdots & \cdots & \vdots \\ N_{OZ-1,1,Z}^\alpha & N_{OZ-1,2,Z}^\alpha & \cdots & N_{OZ-1,E,Z}^\alpha & N_{OZ-1,E+1,Z+1}^\alpha & \cdots & N_{OZ-1,E*\Lambda,F}^\alpha \\ N_{OZ,1,Z}^\alpha & N_{OZ,2,Z}^\alpha & \cdots & N_{OZ,E,Z}^\alpha & N_{OZ,E+1,Z+1}^\alpha & \cdots & N_{OZ,E*\Lambda,F}^\alpha \end{pmatrix} \quad (12)$$

Note that index t is changed after every E^{th} pixel as these are total entries on front side of cube (size $\sqrt{E} \times \sqrt{E}$). K-means++ clustering is then applied on these cubes and clusters are denoised using (6) (cubes are vectorized in this case). After denoising these cubes are projected onto pixels by averaging and converted back to RGB color space.

3. Results and Discussion

The proposed and state-of-the-art existing Poisson denoising techniques are applied on various astronomical images/videos (taken using Hubble telescope). For images, the proposed technique is compared with K-SVD [15], CBM3D [16], PLOW [17], Anscombe transform [18], and NLPCA [5]. The results on videos are compared with KSVD-3D [12], CBM4D [13], and PURE-LET [19].

Figures 1–3 show visual comparison of existing and proposed techniques on three astronomical images (Disk, Nebula, and Jupiter) with different noise peaks. It can be observed that the proposed technique is able to reconstruct a better output image as compared to existing techniques (even in low noise peak values). Tables 1 and 2 provide quantitative analysis of existing and proposed techniques using Peak Signal to Noise Ratio (PSNR) and Structural Similarity Index Measure (SSIM) [20]. Note that the proposed technique provides better quantitative values as compared to the state-of-the-art existing techniques.

Figure 4 shows denoising result of proposed and existing techniques with cube size $20 \times 20 \times 3$ and noise peak = 1. The reconstructed frames (in Figures 4(i) and 4(j)) using

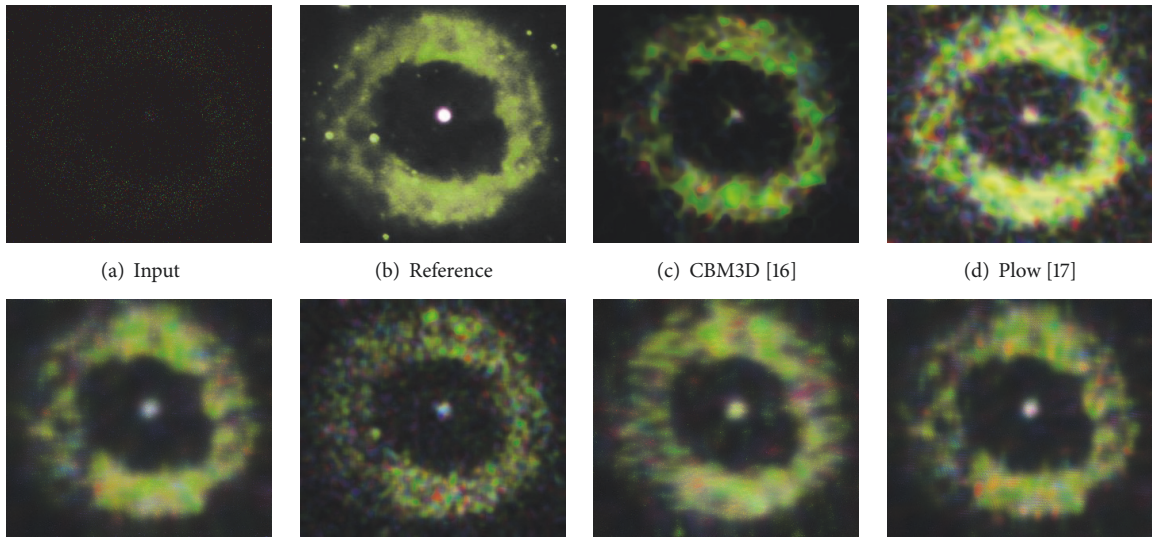

(a) Input (b) Reference (c) CBM3D [16] (d) Plow [17]

(e) Anscombe [18] (f) K-SVD [15] (g) NLPCA [5] (h) Proposed

Figure 2: Nebula: noisy input, reference, and denoised images (for peak = 0.2).

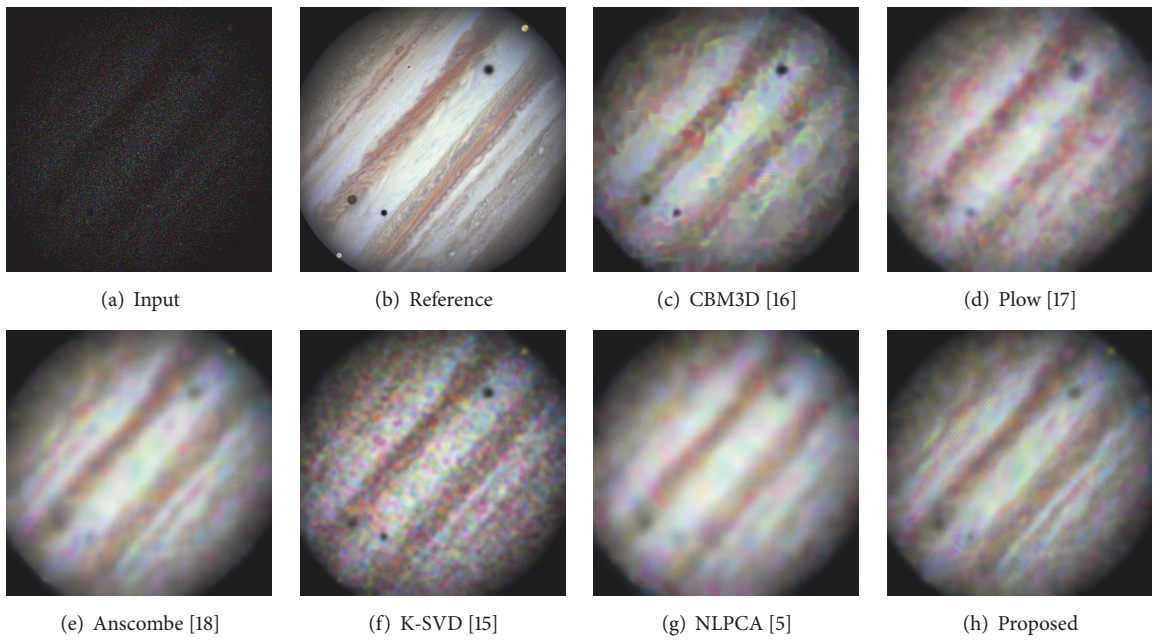

(a) Input (b) Reference (c) CBM3D [16] (d) Plow [17]

(e) Anscombe [18] (f) K-SVD [15] (g) NLPCA [5] (h) Proposed

Figure 3: Jupiter: noisy input, reference, and denoised images (for peak = 1).

Table 1: PSNR comparison.

Techniques	Peak = 0.2			Peak = 0.6			Peak = 1		
	Disk	Infrared	Jupiter	Disk	Nebula	Jupiter	Disk	Nebula	Jupiter
K-SVD [15]	17.766	19.134	12.750	20.001	22.872	16.997	22.961	23.964	20.278
CBM3D [16]	16.905	20.596	16.59	19.989	21.361	19.243	23.331	22.008	22.205
Plow [17]	20.410	17.135	19.50	23.165	20.674	21.091	24.251	23.767	23.04
Anscombe [18]	18.931	21.072	15.818	23.242	23.521	18.742	25.799	23.889	21.112
NLPCA [5]	21.844	23.216	19.705	24.129	22.172	22.379	26.737	24.801	24.212
Proposed	**22.198**	**24.081**	**20.392**	**25.032**	**24.689**	**22.614**	**27.015**	**25.036**	**24.627**

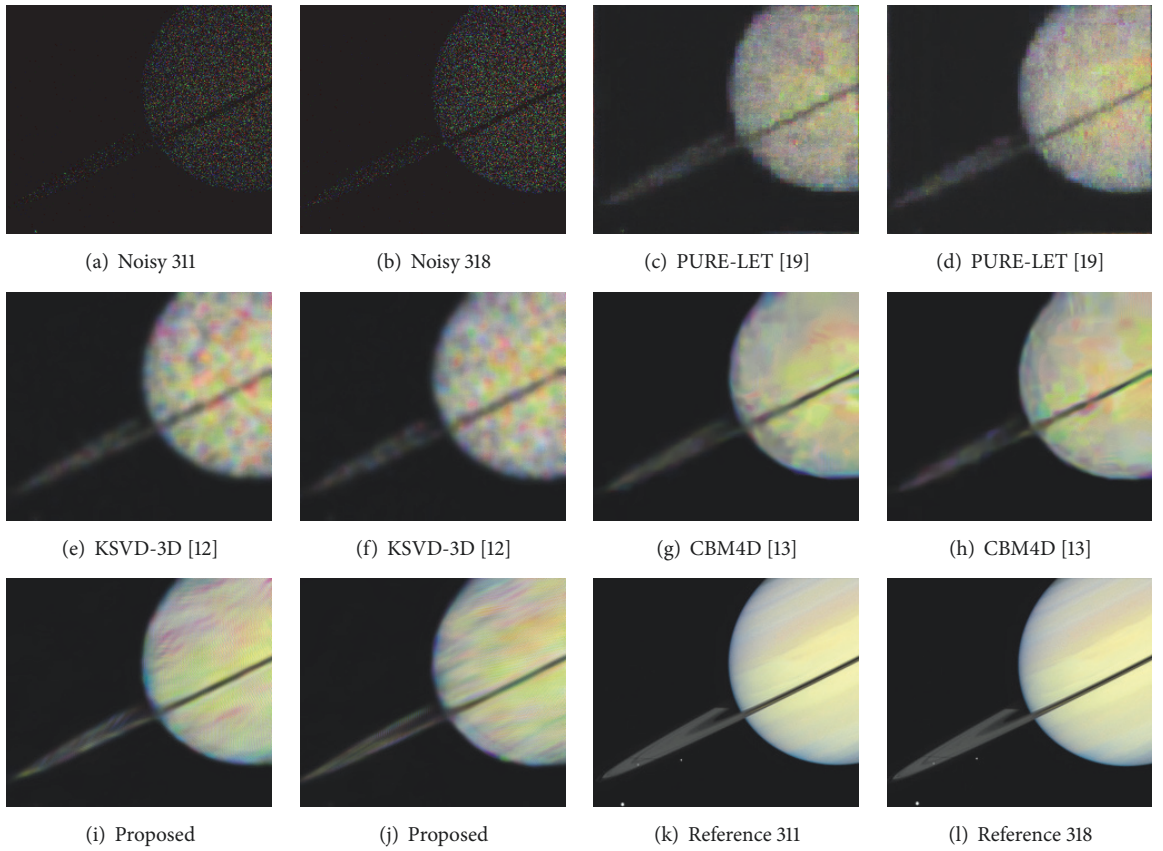

(a) Noisy 311 (b) Noisy 318 (c) PURE-LET [19] (d) PURE-LET [19]

(e) KSVD-3D [12] (f) KSVD-3D [12] (g) CBM4D [13] (h) CBM4D [13]

(i) Proposed (j) Proposed (k) Reference 311 (l) Reference 318

Figure 4: Frames 311 and 318 of a Saturn video.

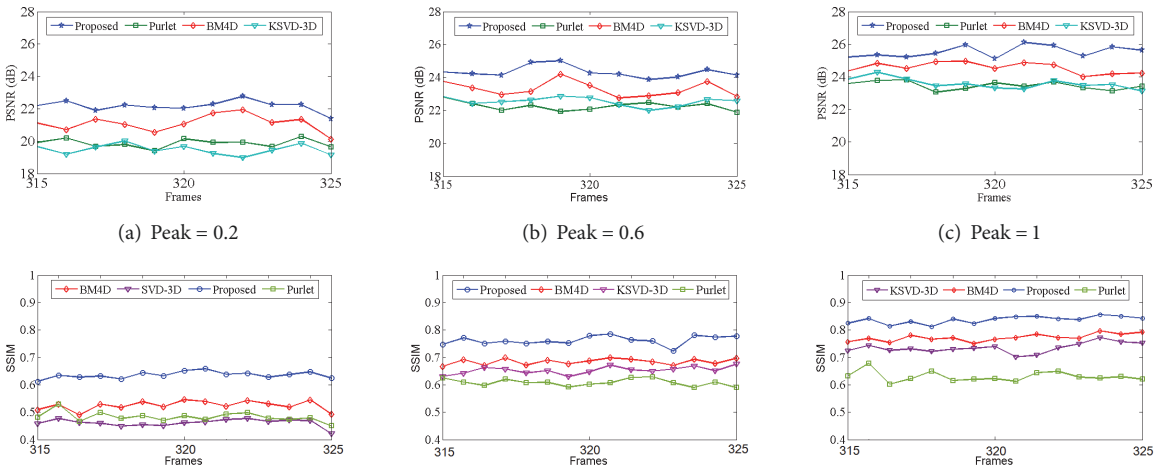

(a) Peak = 0.2 (b) Peak = 0.6 (c) Peak = 1

(d) Peak = 0.2 (e) Peak = 0.6 (f) Peak = 1

Figure 5: (a)–(c) PSNR graphs for peaks 0.2, 0.6, and 1; (d)–(f) SSIM graphs for peaks 0.2, 0.6, and 1.

proposed technique are quite similar to the reference frames (in Figures 4(k) and 4(l)). Figure 5 shows the PSNR and SSIM values of individual frames for different noise peaks. It can be observed that the proposed technique provides better quantitative values almost for all frames as compared to the state-of-the-art existing techniques. Table 3 shows the average quantitative results (PSNR and SSIM) of video frames (311–325). For Figure 5, the Saturn video created from Hubble images taken over about 9-hour span is used. Note that the PSNR and SSIM of only 10 frames (from 315 to 325) are shown in the paper, as scenes in video do not change much due to slow motion of Saturn. Consequently, the PSNR and SSIM values of frames are almost constant.

Table 2: SSIM comparison.

Techniques	Peak = 0.2			Peak = 0.6			Peak = 1		
	Disk	Infrared	Jupiter	Disk	Nebula	Jupiter	Disk	Nebula	Jupiter
K-SVD [15]	0.661	0.495	0.362	0.625	0.579	0.428	0.826	0.756	0.569
CBM3D [16]	0.519	0.556	0.451	0.623	0.692	0.525	0.775	0.787	0.645
PLOW [17]	0.732	0.457	0.356	0.779	0.589	0.509	0.839	0.722	0.635
Anscombe [18]	0.731	0.660	0.469	0.774	0.668	0.584	0.844	0.785	0.661
NLPCA [5]	0.752	0.669	0.476	0.788	0.818	0.571	0.853	0.825	0.683
Proposed	**0.796**	**0.681**	**0.491**	**0.812**	**0.699**	**0.599**	**0.862**	**0.839**	**0.698**

Table 3: Average PSNR (dB) and SSIM values of 311–325 frames.

Techniques	PSNR			SSIM		
	Peak = 0.2	**Peak = 0.6**	**Peak = 1**	**Peak = 0.2**	**Peak = 0.6**	**Peak = 1**
KSVD-3D [12]	19.428	22.286	23.718	0.4621	0.6381	0.7221
CBM4D [13]	21.341	23.644	24.692	0.5211	0.6766	0.7620
PURE-LET [19]	20.055	22.145	23.417	0.4892	0.6212	0.6121
Proposed	**22.426**	**24.534**	**25.528**	**0.6252**	**0.7599**	**0.8312**

4. Conclusion

A Poisson denoising scheme in nonlocal framework using EPCA based on the approach of Gaussian mixture models is proposed for astronomical imaging. The images patches sparsity and dictionary learning approach are unified. The method employs EPCA (which is more suitable for Poisson noise). The scheme first converts the color space from RGB to YCbCr and applies K-means++ clustering on of luminance component only. The same cluster centers are used for chromatic components to improve the computational efficiency. The cubes (in case of color videos) of luminance components (information of both spatial and temporal correlations) are used for improved denoising. Simulation results verify the significance of proposed scheme in both visual and quantitative manner.

Data Availability

The data (images/videos) used in the paper can be provided on demand.

Conflicts of Interest

The authors declare no conflicts of interest regarding publication of this article.

References

[1] P. Fryzlewicz and G. P. Nason, "A Haar-Fisz algorithm for Poisson intensity estimation," *Journal of Computational and Graphical Statistics*, vol. 13, no. 3, pp. 621–638, 2004.

[2] M. Jansen, "Multiscale Poisson data smoothing," *Journal of the Royal Statistical Society: Series B (Statistical Methodology)*, vol. 68, no. 1, pp. 27–48, 2006.

[3] B. Zhang, J. M. Fadili, and J.-L. Starck, "Wavelets, ridgelets, and curvelets for Poisson noise removal," *IEEE Transactions on Image Processing*, vol. 17, no. 7, pp. 1093–1108, 2008.

[4] M. Makitalo and A. Foi, "A closed-form approximation of the exact unbiased inverse of the Anscombe variance-stabilizing transformation," *IEEE Transactions on Image Processing*, vol. 20, no. 9, pp. 2697-2698, 2011.

[5] J. Salmon, Z. Harmany, C.-A. Deledalle, and R. Willett, "Poisson noise reduction with non-local PCA," *Journal of Mathematical Imaging and Vision*, vol. 48, no. 2, pp. 279–294, 2014.

[6] R. Giryes and M. Elad, "Sparsity based Poisson denoising," in *Proceedings of the 2012 IEEE 27th Convention of Electrical and Electronics Engineers in Israel, IEEEI 2012*, isr, November 2012.

[7] W. Cheng and K. Hirakawa, "Minimum risk wavelet shrinkage operator for Poisson image denoising," *IEEE Transactions on Image Processing*, vol. 24, no. 5, pp. 1660–1671, 2015.

[8] A. Mansouri, F. Deger, M. Pedersen, J. Y. Hardeberg, and Y. Voisin, "An adaptive spatial–spectral total variation approach for Poisson noise removal in hyperspectral images," *Signal, Image and Video Processing*, vol. 10, no. 3, pp. 447–454, 2016.

[9] Z. Chen and S. Muramatsu, "Poisson denoising with multiple directional lots," in *Proceedings of the ICASSP 2014 - 2014 IEEE International Conference on Acoustics, Speech and Signal Processing (ICASSP)*, pp. 1225–1229, Florence, Italy, May 2014.

[10] X. Jin, Z. Xu, and K. Hirakawa, "Noise parameter estimation for Poisson corrupted images using variance stabilization transforms," *IEEE Transactions on Image Processing*, vol. 23, no. 3, pp. 1329–1339, 2014.

[11] M. Collins, S. Dasgupta, and R. E. Schapire, "A generalization of principal component analysis to the exponential family," in *Proceedings of the 15th Annual Neural Information Processing Systems Conference, NIPS 2001*, pp. 617–624, December 2001.

[12] M. Protter and M. Elad, "Image sequence denoising via sparse and redundant representations," *IEEE Transactions on Image Processing*, vol. 18, no. 1, pp. 27–35, 2009.

[13] M. Maggioni, G. Boracchi, A. Foi, and K. Egiazarian, "Video denoising, deblocking, and enhancement through separable 4-D nonlocal spatiotemporal transforms," *IEEE Transactions on Image Processing*, vol. 21, no. 9, pp. 3952–3966, 2012.

[14] G. J. Gordon, "Generalized 2 linear 2 models," *Advances in Neural Information Processing Systems*, pp. 577–584, 2002.

[15] L. N. Smith and M. Elad, "Improving dictionary learning: Multiple dictionary updates and coefficient reuse," *IEEE Signal Processing Letters*, vol. 20, no. 1, pp. 79–82, 2013.

[16] K. Dabov, A. Foi, V. Katkovnik, and K. Egiazarian, "Color image denoising via sparse 3D collaborative filtering with grouping constraint in luminance-chrominance space," in *Proceedings of the IEEE International Conference on Image Processing*, pp. 313–316, San Ontonio, Tex, USA, 2007.

[17] P. Chatterjee and P. Milanfar, "Patch-based near-optimal image denoising," *IEEE Transactions on Image Processing*, vol. 21, no. 4, pp. 1635–1649, 2012.

[18] M. Makitalo and A. Foi, "Optimal inversion of the Anscombe transformation in low-count Poisson image denoising," *IEEE Transactions on Image Processing*, vol. 20, no. 1, pp. 99–109, 2011.

[19] F. Luisier, C. Vonesch, T. Blu, and M. Unser, "Fast interscale wavelet denoising of Poisson-corrupted images," *Signal Processing*, vol. 90, no. 2, pp. 415–427, 2010.

[20] Z. Wang, A. C. Bovik, H. R. Sheikh, and E. P. Simoncelli, "Image quality assessment: from error visibility to structural similarity," *IEEE Transactions on Image Processing*, vol. 13, no. 4, pp. 600–612, 2004.